New Insights into the Nucleon's Electromagnetic Structure

Yong-Hui Lin,[1] Hans-Werner Hammer,[2,3] and Ulf-G. Meißner[1,4,5]

[1]Helmholtz Institut für Strahlen- und Kernphysik and Bethe Center for Theoretical Physics, Universität Bonn, D-53115 Bonn, Germany
[2]Department of Physics, Technische Universität Darmstadt, 64289 Darmstadt, Germany
[3]Extreme Matter Institute EMMI and Helmholtz Forschungsakademie Hessen für FAIR (HFHF), GSI Helmholtzzentrum für Schwerionenforschung GmbH, 64291 Darmstadt, Germany
[4]Institute for Advanced Simulation and Institut für Kernphysik, Forschungszentrum Jülich, D-52425 Jülich, Germany
[5]Tbilisi State University, 0186 Tbilisi, Georgia

(Received 8 October 2021; accepted 18 January 2022; published 3 February 2022)

We present a combined analysis of the electromagnetic form factors of the nucleon in the space- and timelike regions using dispersion theory. Our framework provides a consistent description of the experimental data over the full range of momentum transfer, in line with the strictures from analyticity and unitarity. The statistical uncertainties of the extracted form factors are estimated using the bootstrap method, while systematic errors are determined from variations of the spectral functions. We also perform a high-precision extraction of the nucleon radii and find good agreement with previous analyses of spacelike data alone. For the proton charge radius, we find $r_E^p = 0.840^{+0.003\ +0.002}_{-0.002\ -0.002}$ fm, where the first error is statistical and the second one is systematic. The Zemach radius and third moment are in agreement with Lamb shift measurements and hyperfine splittings. The combined dataset of space- and timelike data disfavors a zero crossing of $\mu_p G_E^p/G_M^p$ in the spacelike region. Finally, we discuss the status and perspectives of modulus and phase of the form factors in the timelike region in the context of future experiments, as well as the onset of perturbative QCD.

DOI: 10.1103/PhysRevLett.128.052002

Our everyday matter consists of electrons, protons, and neutrons, with the latter two accounting for essentially all of its mass. While the electron is an elementary particle, protons (p) and neutrons (n), which are collectively referred to as nucleons (N), arise from the complicated strong interaction dynamics of quarks and gluons in quantum chromodynamics (QCD) [1,2]. The electromagnetic (EM) form factors of the nucleon describe the structure of the nucleon as seen by an electromagnetic probe. As such, they provide a window on the strong interaction dynamics in the nucleon over a large range of momentum transfers. For recent reviews see, e.g., Refs. [3–5]. Moreover, they are an important ingredient in the description of a wide range of observables ranging from the Lamb shift in atomic physics [6–9] over the strangeness content of the nucleon [10,11] to the EM structure and reactions of atomic nuclei [12–14]. At small momentum transfers, they are sensitive to the gross properties of the nucleon, like the charge and magnetic moment, as well as the radii. At large momentum transfer, they probe the quark substructure of the nucleon as described by QCD.

Most discussions of nucleon structure focus on the so-called spacelike region, which is accessible via the Lamb shift or elastic electron scattering off the nucleon ($e^- N \to e^- N$), where the four-momentum transfer to the nucleon is spacelike. However, crossing symmetry connects elastic electron scattering to the creation of nucleon-antinucleon pairs in e^+e^- annihilation and its reverse reaction ($e^+e^- \leftrightarrow N\bar{N}$). Both types of processes are described by the Dirac and Pauli form factors F_1 and F_2. They depend on the four-momentum transfer squared t, which is defined in the complex plane. The experimentally accessible spacelike ($t < 0$) and timelike regions [$t > (2m)^2$, with $m = 938.9$ MeV the nucleon mass] on the real axis are connected by an analytic continuation. Experimental data are usually given for the Sachs form factors G_E and G_M, which are linear combinations of F_1 and F_2 and have a physical interpretation in terms of the distribution of charge and magnetization, respectively (see Supplemental Material [15] for details). Note that, in the timelike region, the form factors are complex-valued functions.

The framework of dispersion theory allows us to exploit this link between the space- and timelike data through a combined analysis of experimental data in both regions, fully consistent with the fundamental requirements of

unitarity and analyticity. Building upon our previous analyses of spacelike data only [39,40], we explore this powerful connection and highlight its consequences for the nucleon radii, the behavior of the proton form factor ratio $\mu_p G_E^p/G_M^p$, and the onset of perturbative QCD (pQCD), as well as the modulus and phase of the form factors in the timelike region. In particular, we discuss the implications of the timelike data for the "proton radius puzzle" [41], an apparent discrepancy between the proton radius extracted from the Lamb shift in muonic hydrogen and the value extracted from electron scattering and the electronic Lamb shift; see, e.g., Refs. [42,43] for the current status of this puzzle. It is also important to stress that, in the timelike region, the measured cross section data show an interesting and unexpected oscillatory behavior [44,45].

The matrix element for the creation of a nucleon-antinucleon pair from the vacuum by the EM vector current j_μ^{EM} can be expressed as

$$\langle N(p')\bar{N}(\bar{p}')|j_\mu^{\mathrm{EM}}(0)|0\rangle = \bar{u}(p')\left[F_1(t)\gamma_\mu + i\frac{F_2(t)}{2m}\sigma_{\mu\nu}(p'+\bar{p}')^\nu\right]v(\bar{p}'), \quad (1)$$

where p' and $\bar{p}'$ are the momenta of the nucleon-antinucleon pair and $t=(p'+\bar{p}')^2>0$ is the four-momentum transfer squared. The analytic structure of this matrix element can be discerned by using the optical theorem. Inserting a complete set of intermediate states $|\lambda\rangle$, one finds [46,47]

$$\mathrm{Im}\langle N(p')\bar{N}(\bar{p}')|j_\mu^{\mathrm{EM}}(0)|0\rangle \propto \sum_\lambda \langle N(p')\bar{N}(\bar{p}')|\lambda\rangle \times \langle\lambda|j_\mu^{\mathrm{EM}}(0)|0\rangle\delta^{(4)}(p'+\bar{p}'-p_\lambda). \quad (2)$$

Thus, the imaginary part of the form factors can be related to the matrix element for creation of the intermediate states and the matrix element for scattering of the intermediate states into a $N\bar{N}$ pair. The states $|\lambda\rangle$ must carry the same quantum numbers as the current j_μ^{EM}, i.e., $I^G(J^{PC})=0^-(1^{--})$ for the isoscalar component and $I^G(J^{PC})=1^+(1^{--})$ for the isovector component. Here, I, G, J, P, and C denote the isospin, G parity, spin, parity, and charge conjugation quantum numbers, in order. For the isoscalar (s) part with $I=0$, the lowest mass states are $3\pi, 5\pi, \ldots$; for the isovector (v) part with $I=1$, they are $2\pi, 4\pi, \ldots$. Associated with each intermediate state is a branch cut starting at the corresponding threshold in t and running to infinity.

This analytic structure can be exploited to reconstruct the full form factor from its imaginary part given by Eq. (2). Let $F(t)$ be a generic symbol for one of the nucleon form factors F_1 and F_2. Applying Cauchy's theorem to $F(t)$, we obtain a dispersion relation,

$$F(t)=\lim_{\epsilon\to 0^+}\frac{1}{\pi}\int_{t_0}^{\infty}\frac{\mathrm{Im}F(t')}{t'-t-i\epsilon}dt', \quad (3)$$

which relates the form factor to an integral over its imaginary part ImF. Of course, the derivation assumes that the integral in Eq. (3) converges. This is the case for our parametrization of ImF (see Supplemental Material [15]). We note that a once-subtracted dispersion relation does not improve the form factor description [48].

The longest-range and, therefore, at low momentum transfer, most important continuum contribution to the spectral function Im$F(t)$ comes from the 2π intermediate state, which contributes to the isovector form factors [49]. The ρ appears naturally as a resonance in the 2π continuum with a prominent continuum enhancement on its left wing. A novel and very precise calculation of this contribution has recently been performed in Ref. [50] including the state-of-the-art pion-nucleon scattering amplitudes from dispersion theory [51]. In the isoscalar channel, the nominally longest-range 3π contribution shows no such enhancement and is well accounted for by the ω pole [52,53]. The most important isoscalar continuum contributions are the $K\bar{K}$ [54,55] and $\rho\pi$ continua [56] in the mass region of the ϕ, which is also included as an explicit pole. The remaining contributions to the spectral function above $t\approx 1$ GeV^2 can be parametrized by effective vector meson poles that are fitted to the form factor and cross section data. Since the analytical continuation from the space- to the timelike region is, strictly speaking, an ill-posed problem, the general strategy is to include as few effective poles as possible to describe the data in order to improve the stability of the fit [57].

The number of parameters is reduced by applying various constraints. The asymptotic behavior of the form factors at large spacelike momentum transfer is constrained by perturbative QCD [58]. The power behavior of the form factors leads to superconvergence relations, which reduce the number of fit parameters. Moreover, we constrain the fits to reproduce the high-precision determination of the neutron charge radius squared based on a chiral effective field theory analysis of electron-deuteron scattering [59], $\langle r_n^2\rangle=-0.105^{+0.005}_{-0.006}$ fm^2. All other radii are extracted from the analysis of the data. A detailed discussion of the spectral function is given in the Supplemental Material [15].

The datasets included in our fits are listed in Table I. The first five rows contain spacelike data obtained in elastic electron scattering. Explicit references can be found in the review [40]. In the last four rows, we list the timelike datasets (see [15] for explicit references). The total number of data points in our analysis is 1753.

We have started with fits to the timelike data only. Since the separation of G_E and G_M requires differential cross sections, most timelike data are given for the so-called effective form factor

TABLE I. Datasets included in the combined space- and timelike fits. See Ref. [40] and the Supplemental Material [15] for explicit references.

Data type	Range of $\lvert t\rvert$ (GeV^2)	Number of data
$\sigma(E,\theta)$, PRad	0.000 215–0.058	71
$\sigma(E,\theta)$, MAMI	0.003 84–0.977	1422
$\mu_p G_E^p/G_M^p$, JLab	1.18–8.49	16
G_E^n, world	0.14–1.47	25
G_M^n, world	0.071–10.0	23
$\lvert G_{\rm eff}^p\rvert$, world	3.52–20.25	153
$\lvert G_{\rm eff}^n\rvert$, world	3.53–9.49	27
$\lvert G_E/G_M\rvert$, *BABAR*	3.52–9.0	6
$d\sigma/d\Omega$, BESIII	1.88^2–1.95^2	10

$$|G_{\rm eff}| \equiv \sqrt{\frac{|G_E|^2 + \xi|G_M|^2}{1+\xi}}, \tag{4}$$

with $\xi = t/(2m^2)$. However, there are also some data for the ratio $|G_E/G_M|$ and some differential cross section data from *BABAR* and BESIII. The phase of the ratio G_E/G_M has not been measured. It turns out that a certain number of broad poles above threshold is needed to get a good description of the timelike data. These poles generate the imaginary part of the form factors above the two-nucleon threshold and are required to describe the observed oscillatory behavior of the form factors from *BABAR* and BESIII. With $3s+3v$ below-threshold narrow poles and $3s+3v$ above-threshold broad poles, we were able to obtain a good fit to the data with $\chi^2/\text{d.o.f.} = 0.638$ (where d.o.f. represents degrees of freedom). In particular, the visible strong enhancement of the proton and the neutron timelike form factor (after subtraction of the electromagnetic final-state interaction in the proton case), first seen by the PS170 Collaboration at LEAR [60], is also described in this framework.

In the next step, we include the spacelike data and aim for a consistent analysis of both types of data. We explicitly enforce a decreasing behavior of $G_M^n/(\mu_n G_{\rm dip})$ and $\mu_p G_E^p/G_M^p$ at large $|t|$ in the spacelike region in order to get a good description over the full range of momentum transfers. Moreover, the weight of the timelike ratio $|G_E/G_M|$ data from *BABAR* is increased by a factor of 10 so as to make its contribution to the total χ^2 that is highly suppressed by the large uncertainties more sizable. Stated differently, the factor 10 allows $|G_E/G_M|$ to be constrained properly by the *BABAR* data, but it does not change other quantities, e.g., the proton charge radius is only modified in its fourth digit, well within the theoretical errors, when this factor is set to one.

In Fig. 1, we show our best fit compared to the experimental data for $|G_{\rm eff}|$ of the proton (upper panel) and the neutron (lower panel). Note that this best fit

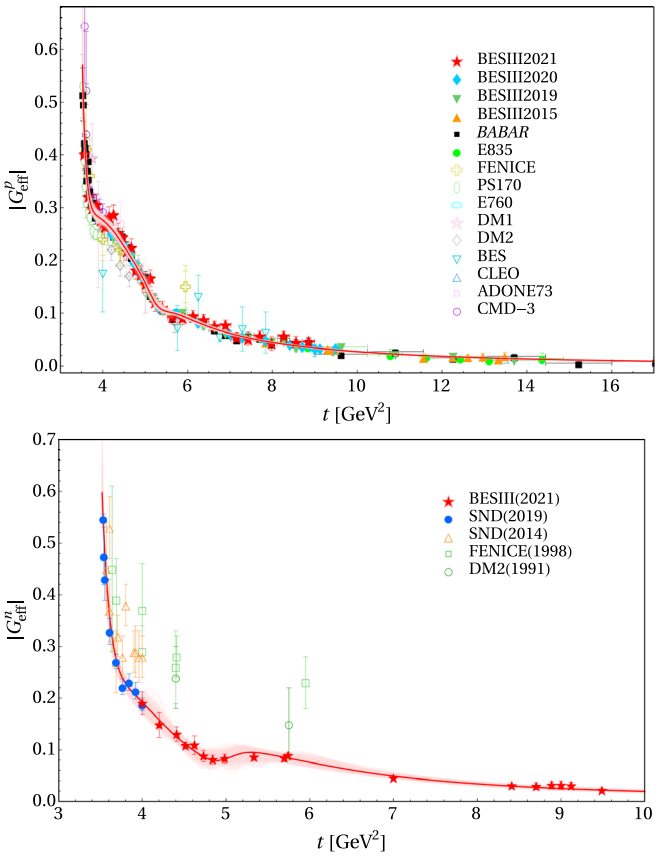

FIG. 1. Complete fit to space- and timelike data with bootstrap error (shaded band) compared to data for $|G_{\rm eff}|$ of the proton (upper) and neutron (lower). Fitted data are depicted by closed symbols; data given by open symbols are shown for comparison only (see Supplemental Material [15] for explicit references).

contains $3s+5v$ below-threshold narrow poles and $3s+3v$ above-threshold broad poles. We obtain a good description of the timelike data for $|G_{\rm eff}|$. The prominent oscillations in $|G_{\rm eff}|$ between the threshold at $t = 4m^2$ and $t \approx 6$ GeV^2 are reproduced by the effective broad poles above threshold. These poles also generate the imaginary part of the form factors in the physical region. Alternatively, these structures can also be generated by including contributions from triangle diagrams with $\Delta\bar{\Delta}$ and $(\Delta\bar{N} + \text{H.c.})$ intermediate states; see, e.g., Ref. [61]. In principle, these contributions are fixed. However, the corresponding coupling constants are poorly known and a perturbative treatment of these contributions is questionable. For further discussion, see Ref. [62].

The quality of the fit to the spacelike data is comparable to our previous fits of spacelike data only [39,40]. We obtain $\chi^2/\text{d.o.f.} = 1.223$ for the full dataset, $\chi^2/\text{d.o.f.} = 1.063$ for the timelike data, and $\chi^2/\text{d.o.f.} = 1.297$ for the spacelike data. Thus, it is warranted to extract the nucleon radii from our combined fit, which has a larger database than spacelike only fits. We obtain the radii

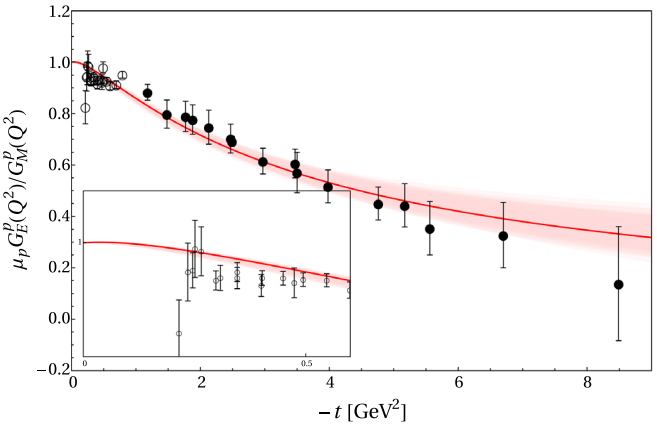

FIG. 2. Complete fit to space- and timelike data with bootstrap error (shaded band) compared to JLab data for $\mu_p G_E^p/G_M^p$ at spacelike momentum transfer. Fitted data are depicted by closed symbols. The data for $|t| < 1$ GeV^2 (open symbols, see also the inset) are shown for comparison only. For references to the data, see Supplemental Material [15].

$$r_E^p = 0.840^{+0.003\ +0.002}_{-0.002\ -0.002}\ \text{fm},$$
$$r_M^p = 0.849^{+0.003\ +0.001}_{-0.003\ -0.004}\ \text{fm},$$
$$r_M^n = 0.864^{+0.004\ +0.006}_{-0.004\ -0.001}\ \text{fm}, \tag{5}$$

where the first error is statistical (based on the bootstrap procedure explained in [15], which leads to the same results as a Bayesian analysis [40]) and the second one is systematic (based on the variations in the spectral functions, see [15]). These values are in good agreement with previous high-precision analyses of spacelike data alone [39,40] and have comparable errors. For the Zemach radius r_z and the third Zemach moment $\langle r^3 \rangle_{(2)}$ (see Supplemental Material [15]), we obtain

$$r_z = 1.054^{+0.003\ +0.000}_{-0.002\ -0.001}\ \text{fm},$$
$$\langle r^3 \rangle_{(2)} = 2.310^{+0.022\ +0.014}_{-0.018\ -0.015}\ \text{fm}^3. \tag{6}$$

These values are in good agreement with Lamb shift and hyperfine splittings in muonic hydrogen [63].

Another interesting question in the spacelike region concerns the behavior of the form factor ratio $\mu_p G_E^p/G_M^p$ for intermediate momentum transfer. Some measurements suggest a zero crossing of this ratio around $t \approx -10$ GeV^2 [64]. In Fig. 2, we compare our fit to the experimental data for $\mu_p G_E^p/G_M^p$. While we obtain a good description of the data, a zero crossing is disfavored by the combined analysis of space- and timelike data. Thus, data at higher momentum transfer than shown in the figure are required to settle this issue. We further remark that, as in the earlier fits to the spacelike data only, the onset of perturbative QCD barely sets in at the highest momentum transfers probed.

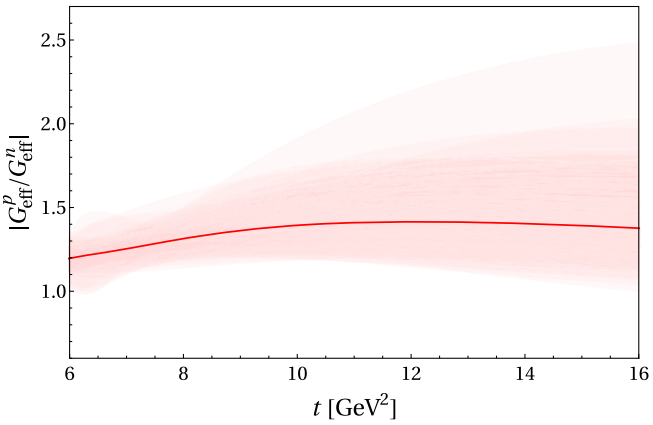

FIG. 3. Form factor ratio $|G_{\text{eff}}^p(t)/G_{\text{eff}}^n(t)|$ in the timelike region for the best fit, with the bootstrap uncertainties indicated by the shaded band.

Based on quark counting rules [58], the form factor ratio $|G_{\text{eff}}^p(t)/G_{\text{eff}}^n(t)|$ should approach a constant as $t \to \infty$ in the timelike region. We show our result for this ratio in Fig. 3. The form factor ratio is constant above $t \simeq 6$ GeV^2 and slightly larger than 1, with sizeable uncertainties for

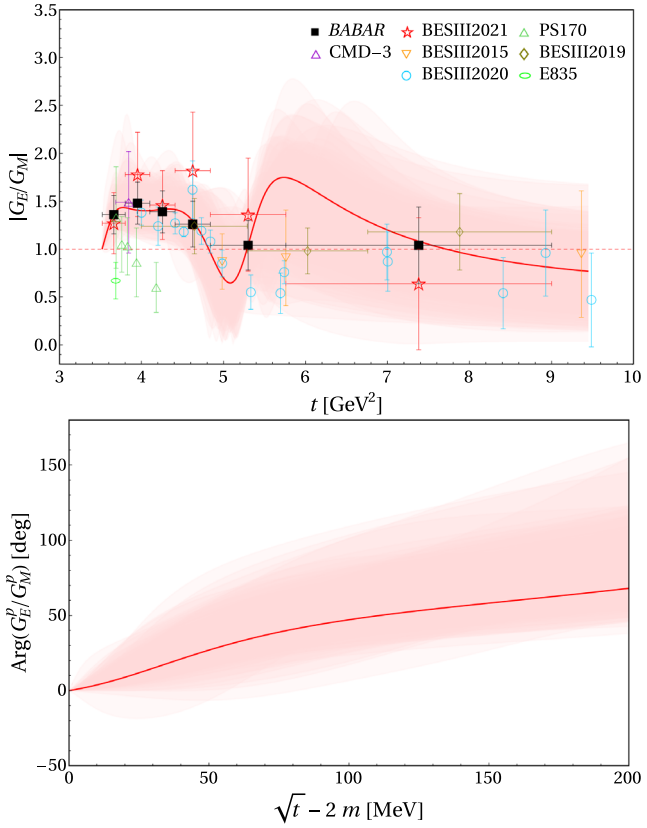

FIG. 4. Complete fit to space- and timelike data with bootstrap error (shaded band) compared to proton data for $|G_E/G_M|$ (closed symbols, fitted; open symbols, not fitted) (upper) and our prediction for $\arg(G_E/G_M)$ (lower).

$t > 10\ \mathrm{GeV}^2$. However, drawing a clear conclusion about the onset of pQCD certainly requires the separated form factors G_E and G_M, and not just the effective form factor.

In addition to $|G_{\mathrm{eff}}|$, there are also data on the ratio $|G_E/G_M|$ and on differential cross sections for the proton in the timelike region. The differential cross sections from BESIII in the lowest energy bin ($t \in [1.877, 1.950]\ \mathrm{GeV}^2$) are included in our fit and are well described. The corresponding differential cross sections from *BABAR* are also well described, when normalized to the total cross section. In Fig. 4, we compare the fit to the proton data for $|G_E/G_M|$ and give our prediction for the phase of G_E/G_M. We fit only to the *BABAR* data for $|G_E/G_M|$ since the BESIII data have much larger error bars. The modulus $|G_E/G_M|$ is well described by our fit, but the bootstrap errors grow to more than 100% at $t \approx 6\ \mathrm{GeV}^2$. The phase $\arg(G_E/G_M)$ is experimentally unrestricted due to the lack of data and thus has large errors. For energies $\sqrt{t} - 2m$ larger than 200 MeV, it is essentially unconstrained by our fit. Future measurements of the phase such as planned with PANDA at FAIR would be highly valuable to improve this situation [65].

In summary, for the first time, a consistent picture of the nucleons electromagnetic structure based on all spacelike and timelike data from electron scattering and electron-positron annihilation (and its reversed process) emerges. In particular, the extracted proton charge radius $r_E^p = 0.840$ fm is small and consistent with earlier dispersive analyses [40] and most recent determinations from electron-proton scattering as well as the Lamb shift in electronic and muonic hydrogen (as listed, e.g., in Ref. [42]). The Zemach radius and third moment are in agreement with Lamb shift measurements and hyperfine splittings in muonic hydrogen [63]. Still, there are open questions related to the onset of pQCD and the behavior of the form factor ratio $\mu_p G_E^p/G_M^p$ at intermediate $|t|$ in the spacelike region, as well as the precise behavior of this complex-valued ratio in the timelike region. These issues can only be settled by accurate measurements combined with precise analyses as in the framework utilized here.

The work of U.-G. M. and Y.-H. L. is supported in part by the Deutsche Forschungsgemeinschaft (DFG, German Research Foundation) and the NSFC through the funds provided to the Sino-German Collaborative Research Center TRR 110 "Symmetries and the Emergence of Structure in QCD" (DFG Project-ID 196253076—TRR 110, NSFC Grant No. 12070131001), by the Chinese Academy of Sciences (CAS) through a President's International Fellowship Initiative (PIFI) (Grant No. 2018DM0034), by the VolkswagenStiftung (Grant No. 93562), and by the EU Horizon 2020 research and innovation program, STRONG-2020 project under Grant Agreement No. 824093. H.-W. H. was supported by the Deutsche Forschungsgemeinschaft (DFG, German Research Foundation)—Projektnummer 279384907—CRC 1245 and by the German Federal Ministry of Education and Research (BMBF) (Grant No. 05P21RDFNB).

[1] K. G. Wilson, Phys. Rev. D **10**, 2445 (1974).
[2] F. Wilczek, Central Eur. J. Phys. **10**, 1021 (2012).
[3] A. Denig and G. Salme, Prog. Part. Nucl. Phys. **68**, 113 (2013).
[4] S. Pacetti, R. Baldini Ferroli, and E. Tomasi-Gustafsson, Phys. Rep. **550–551**, 1 (2015).
[5] V. Punjabi, C. F. Perdrisat, M. K. Jones, E. J. Brash, and C. E. Carlson, Eur. Phys. J. A **51**, 79 (2015).
[6] R. Pohl *et al.*, Nature (London) **466**, 213 (2010).
[7] A. Beyer *et al.*, Science **358**, 79 (2017).
[8] H. Fleurbaey, S. Galtier, S. Thomas, M. Bonnaud, L. Julien, F. Biraben, F. Nez, M. Abgrall, and J. Guena, Phys. Rev. Lett. **120**, 183001 (2018).
[9] N. Bezginov, T. Valdez, M. Horbatsch, A. Marsman, A. C. Vutha, and E. A. Hessels, Science **365**, 1007 (2019).
[10] D. S. Armstrong and R. D. McKeown, Annu. Rev. Nucl. Part. Sci. **62**, 337 (2012).
[11] F. E. Maas and K. D. Paschke, Prog. Part. Nucl. Phys. **95**, 209 (2017).
[12] S. Bacca and S. Pastore, J. Phys. G **41**, 123002 (2014).
[13] D. R. Phillips, Annu. Rev. Nucl. Part. Sci. **66**, 421 (2016).
[14] H. Krebs, Eur. Phys. J. A **56**, 234 (2020).
[15] See Supplemental Material at http://link.aps.org/supplemental/10.1103/PhysRevLett.128.052002 for further details on form factors, the spectral functions, the fitting procedure and the data base, which includes Refs. [16–38].
[16] M. Ablikim *et al.* (BESIII Collaboration), Phys. Rev. Lett. **124**, 042001 (2020).
[17] M. Ablikim *et al.* (BESIII Collaboration), Phys. Rev. D **99**, 092002 (2019).
[18] M. Ablikim *et al.* (BESIII Collaboration), Phys. Rev. D **91**, 112004 (2015).
[19] M. Ambrogiani, S. Bagnasco, W. Baldini, D. Bettoni, G. Borreani *et al.* (E835 Collaboration), Phys. Rev. D **60**, 032002 (1999).
[20] M. Andreotti, S. Bagnasco, W. Baldini, D. Bettoni, G. Borreani, A. Buzzo, R. Calabrese, R. Cester, G. Cibinetto, and P. Dalpiaz *et al.*, Phys. Lett. B **559**, 20 (2003).
[21] A. Antonelli, R. Baldini, M. Bertani, M. E. Biagini, V. Bidoli, C. Bini, T. Bressani, R. Calabrese, R. Cardarelli, and R. Carlin *et al.*, Phys. Lett. B **313**, 283 (1993).
[22] A. Antonelli, R. Baldini, M. Bertani, M. E. Biagini, V. Bidoli, C. Bini, T. Bressani, R. Calabrese, R. Cardarelli, R. Carlin *et al.*, Phys. Lett. B **334**, 431 (1994).
[23] A. Antonelli, R. Baldini, P. Benasi, M. Bertani, M. E. Biagini, V. Bidoli, C. Bini, T. Bressani, R. Calabrese, R. Cardarelli *et al.*, Nucl. Phys. **B517**, 3 (1998).
[24] T. A. Armstrong *et al.* (E760 Collaboration), Phys. Rev. Lett. **70**, 1212 (1993).
[25] B. Delcourt, I. Derado, J. L. Bertrand, D. Bisello, J. C. Bizot, J. Buon, A. Cordier, P. Eschstruth, L. Fayard, J. Jeanjean *et al.*, Phys. Lett. **86B**, 395 (1979).

[26] D. Bisello, S. Limentani, M. Nigro, L. Pescara, M. Posocco, P. Sartori, J. E. Augustin, G. Busetto, G. Cosme, F. Couchot *et al.*, Nucl. Phys. **B224**, 379 (1983).
[27] D. Bisello *et al.* (DM2 Collaboration), Z. Phys. C **48**, 23 (1990).
[28] M. Ablikim *et al.* (BES Collaboration), Phys. Lett. B **630**, 14 (2005).
[29] T. K. Pedlar *et al.* (CLEO Collaboration), Phys. Rev. Lett. **95**, 261803 (2005).
[30] M. Castellano, G. Di Giugno, J. W. Humphrey, E. Sassi Palmieri, G. Troise, U. Troya, and S. Vitale, Nuovo Cimento A **14**, 1 (1973).
[31] R. R. Akhmetshin *et al.* (CMD-3 Collaboration), Phys. Lett. B **759**, 634 (2016).
[32] M. Ablikim *et al.* (BESIII Collaboration), arXiv:2103.12486.
[33] V. P. Druzhinin and S. I. Serednyakov, EPJ Web Conf. **212**, 07007 (2019).
[34] M. N. Achasov, A. Y. Barnyakov, K. I. Beloborodov, A. V. Berdyugin, D. E. Berkaev, A. G. Bogdanchikov, A. A. Botov, T. V. Dimova, V. P. Druzhinin, V. B. Golubev *et al.*, Phys. Rev. D **90**, 112007 (2014).
[35] M. E. Biagini, E. Pasqualucci, and A. Rotondo, Z. Phys. C **52**, 631 (1991).
[36] S. h. Seo, Ph.D thesis, University of Minnesota, USA, 2004.
[37] M. Ambrogiani *et al.* (Fermilab E835 Collaboration), Phys. Lett. B **610**, 177 (2005).
[38] F. James and M. Roos, Comput. Phys. Commun. **10**, 343 (1975).
[39] Y. H. Lin, H.-W. Hammer, and U.-G. Meißner, Phys. Lett. B **816**, 136254 (2021).
[40] Y. H. Lin, H.-W. Hammer, and U.-G. Meißner, Eur. Phys. J. A **57**, 255 (2021).
[41] J. C. Bernauer and R. Pohl, Sci. Am. **310**, 32 (2014).
[42] H.-W. Hammer and U.-G. Meißner, Sci. Bull. **65**, 257 (2020).
[43] J. P. Karr, D. Marchand, and E. Voutier, Nat. Rev. Phys. **2**, 601 (2020).
[44] J. P. Lees *et al.* (*BABAR* Collaboration), Phys. Rev. D **87**, 092005 (2013).
[45] M. Ablikim *et al.* (BESIII Collaboration), Phys. Lett. B **817**, 136328 (2021).
[46] G. F. Chew, R. Karplus, S. Gasiorowicz, and F. Zachariasen, Phys. Rev. **110**, 265 (1958).
[47] P. Federbush, M. L. Goldberger, and S. B. Treiman, Phys. Rev. **112**, 642 (1958).
[48] C. Krämer, Diploma thesis, University of Bonn, 2009.
[49] W. R. Frazer and J. R. Fulco, Phys. Rev. **117**, 1609 (1960).
[50] M. Hoferichter, B. Kubis, J. Ruiz de Elvira, H.-W. Hammer, and U.-G. Meißner, Eur. Phys. J. A **52**, 331 (2016).
[51] M. Hoferichter, J. Ruiz de Elvira, B. Kubis, and U.-G. Meißner, Phys. Rep. **625**, 1 (2016).
[52] V. Bernard, N. Kaiser, and U.-G. Meißner, Nucl. Phys. **A611**, 429 (1996).
[53] N. Kaiser and E. Passemar, Eur. Phys. J. A **55**, 16 (2019).
[54] H.-W. Hammer and M. J. Ramsey-Musolf, Phys. Rev. C **60**, 045205 (1999); **62**, 049903(E) (2000).
[55] H.-W. Hammer and M. J. Ramsey-Musolf, Phys. Rev. C **60**, 045204 (1999); **62**, 049902(E) (2000).
[56] U.-G. Meißner, V. Mull, J. Speth, and J. W. van Orden, Phys. Lett. B **408**, 381 (1997).
[57] I. Sabba Stefanescu, J. Math. Phys. (N.Y.) **21**, 175 (1980).
[58] G. P. Lepage and S. J. Brodsky, Phys. Rev. D **22**, 2157 (1980).
[59] A. A. Filin, D. Möller, V. Baru, E. Epelbaum, H. Krebs, and P. Reinert, Phys. Rev. C **103**, 024313 (2021).
[60] G. Bardin *et al.*, Nucl. Phys. **B411**, 3 (1994).
[61] I. T. Lorenz, H.-W. Hammer, and Ulf-G. Meißner, Phys. Rev. D **92**, 034018 (2015).
[62] A. Bianconi and E. Tomasi-Gustafsson, Phys. Rev. Lett. **114**, 232301 (2015).
[63] A. Antognini, F. Nez, K. Schuhmann, F. D. Amaro, F. Biraben, J. M. R. Cardoso, D. S. Covita, A. Dax, S. Dhawan, and M. Diepold *et al.*, Science **339**, 417 (2013).
[64] J. Arrington, K. de Jager, and C. F. Perdrisat, J. Phys. Conf. Ser. **299**, 012002 (2011).
[65] A. Dbeyssi (PANDA Collaboration), EPJ Web Conf. **204**, 01004 (2019).